Source-receiver interferometry for seismic wavefield construction and ground-roll removal

CRAIG DUGUID, University of Edinburgh, presently Tullow Oil
DAVID HALLIDAY, Schlumberger Cambridge Research
ANDREW CURTIS, University of Edinburgh

Seismic interferometry describes the construction of unmeasured wavefield responses (or Green's functions) between two or more points by applying cross-correlation, deconvolution, or convolution to seismic data recordings. The practical implications are that, applying inter-receiver interferometry, a "virtual" (imaginary) source of energy can be created at the location to a real receiver by using energy recorded from surrounding sources. Similarly, by using inter-source interferometry, a virtual receiver can be created at the location of a real source by using energy recorded at surrounding receivers (Curtis et al., 2009). These two methods can be combined to create the new technique of source-receiver interferometry (Curtis, 2009; Curtis and Halliday, 2010; Halliday and Curtis, 2010) which synthesizes real-source to real-receiver Green's function estimates using only energy recorded at a surrounding boundary of receivers and from an additional surrounding boundary of sources. The boundary sources in each case can be active (such as an explosive or vibrating source) or passive (such as noise from anthropogenic activity or ocean waves). This paper describes the first real-data application of source-receiver interferometry, and demonstrates its potential to enhance existing methods of interferometric ground-roll suppression.

Exact expressions for the construction of inter-receiver Green's functions by cross-correlation are presented in Wapenaar and Fokkema (2006) and van Manen et al. (2006). For practical reasons, we use a number of approximations to the exact theory of seismic interferometry. To summarize, the equations utilize a high-frequency approximation, assume that the surrounding sources used in the interferometric construction exist on a closed boundary with large radius separated at intervals no greater than that required by the Nyquist spatial sampling criterion, and assume that the medium on and outside the boundary of sources is homogeneous. Under these assumptions and when dealing with sources with unknown power spectra, the following frequency domain expression allows for an estimate of the causal (time forward) and acausal (time reversed) Green's functions between two receiver locations to be obtained. This is achieved by cross-correlating particle velocity measurements at two receivers and integrating the result over each source position on a surface S surrounding both receivers (after Wapenaar and Fokkema, 2006):

$$\mathrm{G}(\mathbf{r}_2,\mathbf{r}_1)+\mathrm{G}^*(\mathbf{r}_2,\mathbf{r}_1)\approx C(\omega)\oint_S v^{obs*}(\mathbf{r}_1,\mathbf{r})\;\; v^{obs}(\mathbf{r}_2,\mathbf{r})\,\mathrm{d}S \qquad (1)$$

Here, $\mathrm{G}(\mathbf{r}_2,\mathbf{r}_1)$ is the Green's function representing the wavefield (particle velocity) at $\mathbf{r}_2$ due to a monopolar point source at $\mathbf{r}_1$, $v^{obs}(\mathbf{r}_2,\mathbf{r})$ is the observed particle velocity at $\mathbf{r}_2$ due to a source at r on S, * denotes complex conjugation and $C(w)$ is an (unknown) frequency-dependent scaling factor. The multiplication of one quantity with the complex conjugate of the other on the right hand side of Equation 1 is equivalent to cross-correlation in the time domain. Complex conjugation in the frequency domain results in time reversal, and hence $\mathrm{G}^*(\mathbf{r}_2,\mathbf{r}_1)$ on the left of Equation 1 is the acausal (time-reversed) Green's function. This means that the result of applying the operations on the right is to produce two Green's functions (or seismograms), both starting from zero time but one extends toward positive times, $\mathrm{G}(\mathbf{r}_2,\mathbf{r}_1)$, while the other extends toward negative times $\mathrm{G}^*(\mathbf{r}_2,\mathbf{r}_1)$.

A similar expression exists for inter-receiver interferometry by convolution:

$$\mathrm{G}(\mathbf{r}_2,\mathbf{r}_1)\approx C(\omega)\oint_S v^{obs}(\mathbf{r}_1,\mathbf{r})\;\; v^{obs}(\mathbf{r}_2,\mathbf{r})\,dS \qquad (2)$$

The application of this expression requires that the source boundary S surrounds only one of the receivers at $\mathbf{r}_1$ and $\mathbf{r}_2$, not both as required for correlation in Equation 1. In the case of convolution in Equation 2, only the acausal Green's function is recovered.

In an extension of the theory for inter-receiver interferometry, exact expressions can be formulated for Green's function retrieval by source-receiver interferometry (Curtis and Halliday, 2010). These exact expressions can be simplified under the same assumptions as for Equations 1 and 2 above to (Curtis and Halliday, 2010):

$$\mathrm{G}^*(\mathbf{r}_2,\mathbf{r}_1)+\mathrm{G}(\mathbf{r}_2,\mathbf{r}_1)\approx C(\omega)\oint_{S_1}\oint_{S_2} v^{obs}(\mathbf{r}',\mathbf{r}_1)\,v^{obs*}(\mathbf{r}',\mathbf{r})\,v^{obs}(\mathbf{r}_2,\mathbf{r})\,dS_2\,dS_1 \qquad (3)$$

An example geometry for the source position $\mathbf{r}_1$, receiver position $\mathbf{r}_2$ and boundaries S_1 (containing sources $\mathbf{r}$) and S_2 (containing receivers $\mathbf{r}'$) is illustrated in Figure 1. This equation allows the wavefield between a real source at $\mathbf{r}_1$ and a real receiver at $\mathbf{r}_2$ to be constructed using interferometry, without actually directly measuring this wavefield. A number of potential applications of source-receiver interferometry to noise removal, quality evaluation of the results of interferometry, and seismic imaging are discussed in Curtis and Halliday (2010), Halliday and Curtis (2010), and Poliannikov (2011). In this paper, we apply inter-receiver interferometry by both cross-correlation and convolution, and also source-receiver interferometry to a shallow land-seismic data set, with the results illustrating the potential of source-receiver interferometry in surface-wave (ground-roll) suppression, allowing the method to be added to the developing suite of interferometric techniques for the removal of ground roll.

Source-receiver interferometry data example

In order to illustrate the application of inter-receiver and

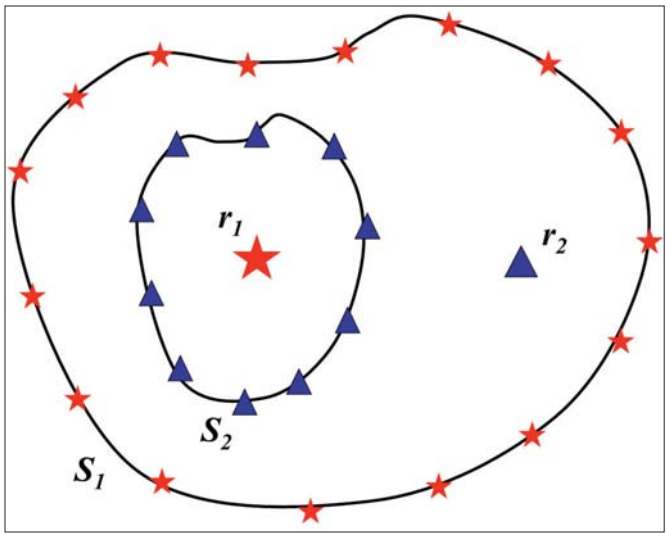

Figure 1. *One canonical geometry for source-receiver interferometry between a real source at* $\mathbf{r}_1$ *and a real receiver at* $\mathbf{r}_2$*. Stars represent sources and triangles represent receivers.*

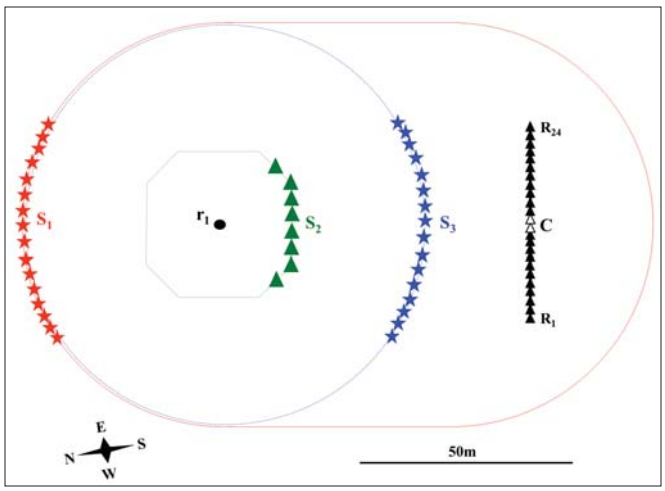

Figure 2. *Survey acquisition geometry. Data recordings exist from a receiver at position* $\mathbf{r}_1$ *(black in-filled circle), receivers on a closed boundary* S_2 *(green stippled line), and on a 24-geophone linear array* (R_1- R_{24}, *black/white triangles) from sources on a running track shaped boundary* S_1 *(red line), a circular boundary* S_3 *(blue line) and from a single source at position* $\mathbf{r}_1$ *(black in-filled circle). In the data examples presented here, only sources and receivers marked by in-filled stars and triangles on boundaries* S_1, S_2, *and* S_3 *have been used in the interferometric constructions. These denoted sources and receivers lie within approximate stationary-phase regions for the considered frequency range.*

source-receiver interferometry, use is made of data acquired at the Schlumberger Cambridge Research Centre. The survey geometry for the experiment is illustrated in Figure 2. Vertical component geophones recording particle velocity were located at position $\mathbf{r}_1$, at 4-m intervals on a convolutional boundary S_2, and at 2-m intervals on a line of 24 geophones oriented approximately east-west and centered at point C (notice that north is approximately to the left in Figure 2). Active shot records from an accelerated weight drop source were made from a source positioned at $\mathbf{r}_1$, from a set of source positions separated by 4-m intervals on the correlational source boundary S_1, and from source positions separated by 4-m intervals on the convolutional boundary S_3. All results plotted herein are either true measured responses or interferometric constructions for receivers on the 24 geophone line and for either a real or a virtual source at location $\mathbf{r}_1$.

Before constructing wavefield responses by interferometry, a number of preprocessing steps were applied to all recorded data. In the first instance, a frequency-dependent transfer function was used to correct the recorded seismic data for discrepancies in the frequency response of the specific geophones used at each location. The procedure converted the responses of the 14-Hz geophones on S_2 and of the 4.5-Hz geophones on the 24 geophone linear array to the response of the 10-Hz geophone at position $\mathbf{r}_1$. Two steps were taken in order to reduce the effect of unwanted low-frequency ambient noise principally generated by vehicles driving on surrounding roads throughout the data acquisition period. Five individual shot records were acquired at each shot location. Following a visual inspection of each shot record, only clean records were stacked to obtain single-shot records, thus maximizing signal-to-noise ratio on records from each shot location. Furthermore, a high-pass filter with corner frequency of 10 Hz has been applied to the entire data set to further suppress this low-frequency noise. The Nyquist frequency for this data set is 125 Hz, thus all results have a bandwidth of 10–125 Hz."

Figure 3 depicts examples of both the preprocessed (real source) waveforms and interferometrically constructed (virtual-source) waveforms for a receiver (C) at the center of the linear array (taken as the average response of the two geophones either side of this central location denoted by white triangles in Figure 2). The black dashed trace in each panel of Figure 3 is the particle velocity measured at point C from an active source at position $\mathbf{r}_1$ (this direct recording is never used in the interferometric Green's function constructions). Higher-frequency (approximately 50–80 Hz) direct and guided body-wave arrivals are evident between 0.05 and 0.2 s arrival time, whereas a strong surface-wave envelope consisting of both fundamental and higher mode surface-waves observed at an arrival time of between 0.6 and 0.9 s. One further significant arrival is observed slightly after 0.4 s arrival time which is identified as a refracted shear-wave arrival. Weak scattered-wave or residual ambient-noise energy is present at arrival times greater than 1 s.

In addition to this directly recorded single shot, three interferometric constructions are presented in Figure 3. The solid red curve in Figure 3a represents the response at point C from a virtual source at position $\mathbf{r}_1$ constructed by applying Equation 1 to data recorded by the receiver at position $\mathbf{r}_1$ and the receivers at C from sources depicted by red stars on S_1 in Figure 2. These sources lie in the approximate stationary-phase region which Snieder (2004) showed was the main contributing part of the source boundary for constructing directly propagating waves in the causal interferometric estimate between a virtual source at $\mathbf{r}_1$ and the receivers at C by cross-correlation. Only the causal (time forward) part of the result has been plotted.

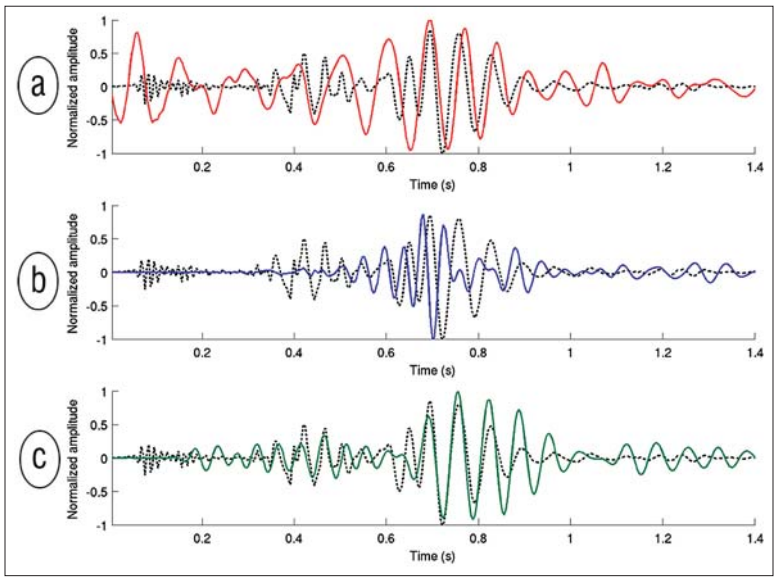

Figure 3. *Colored traces are seismic interferometry results plotted for a receiver at point C in Figure 2, taken as an average of the traces recorded at receivers 12 and 13 on the linear array (white triangles) using a virtual source at position* $\mathbf{r}_1$*. The black dashed trace in each case is the particle velocity measured at point C from an active source at position* $\mathbf{r}_1$*. (a) The causal inter-receiver cross-correlation result (solid red) constructed using data recorded from active sources on boundary* S_1 *denoted by red in-filled stars in Figure 2. (b) The inter-receiver convolution result (solid blue) constructed using data recorded from active sources on boundary* S_3 *denoted by blue in-filled stars in Figure 2. (c) The source-receiver result (solid green) constructed using both data recorded from active sources on boundary* S_1 *denoted by red in-filled stars, and data recorded at receivers on boundary* S_2 *denoted by green triangles in Figure 2. In all cases, a high-pass frequency filter with corner frequency of 10 Hz has been applied before plotting (active source data) and before interferometry.*

The solid blue curve in Figure 3b represents the response at point C from a virtual-source at position $\mathbf{r}_1$ constructed by applying Equation 2 to data recorded at the receiver at position $\mathbf{r}_1$ and the receivers at C from sources depicted by blue in-filled stars on S_3. These sources lie in the approximate stationary-phase region for constructing directly propagating waves in the interferometric estimate between a virtual source at $\mathbf{r}_1$ and the receivers at C by convolution.

Source-receiver interferometry can be applied to the geometry presented in Figure 2 via Equation 3. In practice, application of Equation 3 first involves calculating Green's function estimates between each receiver on the convolutional boundary S_2 and each receiver on the linear array. This is achieved by calculating the response at each receiver on the linear array due to a virtual source created at each receiver location on the convolutional boundary S_2, using sources on the correlational boundary S_1 via for example Equation 1. We then have an estimate of the Green's function between each receiver on S_2 and each receiver on the linear array. To complete the source-receiver interferometry process in Equation 3 for one linear array receiver, we first convolve the response at each given receiver on S_2 from the source at $\mathbf{r}_1$ with the newly constructed response between this receiver on S_2 and the linear array receiver, then integrate the results over all receivers (virtual sources) on the boundary S_2. The result of applying Equation 3, using only data recorded from sources depicted by the red in-filled stars on S_1 and data recorded at the green in-filled triangles on S_2, is shown by the solid green curve in Figure 3c.

Figure 3 shows that each of the three interferometric methods have recovered the directly measured wavefield response (black dashed line) to differing levels of accuracy. In each case, the surface waves (ground roll) are the most identifiable events recovered, with the relative amplitude errors of the source-receiver and inter-receiver correlational results, contrasting with noticeable phase errors in the wavefield recovered by inter-receiver convolutional interferometry. The source-receiver result also appears to be the only one to reconstruct the event with an arrival time of just over 0.4 s; significant nonphysical arrivals (artifacts constructed in the interferometry result which do not correspond to physically propagating waves) present in the inter-receiver cross-correlation result would mask this arrival if it exists there at all. These nonphysical arrivals are constructed when the approximations assumed in the derivation of Equations 1, 2, and 3 are violated. Particularly likely in this example are nonphysical arrivals present in the final result due to using a source boundary which does not extend in depth to include sources within the subsurface of the Earth as required by exact formulations of the theory (see Halliday and Curtis, 2008). In practice, using only the highlighted stationary-phase source and receiver positions on the boundaries inhibits construction of further nonphysical arrivals compared to using the full 2D boundaries shown in Figure 2. The nonphysical arrivals evident in the inter-receiver cross-correlation result (Figure 3a) are a likely cause of the distinct "ringing" pattern in the source-receiver result (Figure 3c). This follows from the fact that the source-receiver expression (Equation 3) also uses a series of wavefields constructed by inter-receiver cross-correlation interferometry, integrated over virtual sources on S_2.

Application to removal of ground roll

One additional difference between the directly measured wavefield response (black dashed line in Figure 3) and each of the interferometrically constructed wavefields is that the high-frequency body waves evident in the directly measured wavefield (principally present between 0.05 and 0.2 s arrival time and noticeably present up to 0.5 s arrival time) have not been substantially recovered by any of the interferometric methods. This fact is again linked to the concept of stationary-phase analysis (Snieder, 2004) which can explain why surface waves are expected to dominate the results of interferometry experiments which utilize sources only on the surface of the medium, i.e., in this case using sources at the Earth's surface only (Halliday et al., 2007; Halliday and Curtis, 2008; Forghani and Snieder, 2010). For this reason, interferometry has been pro-

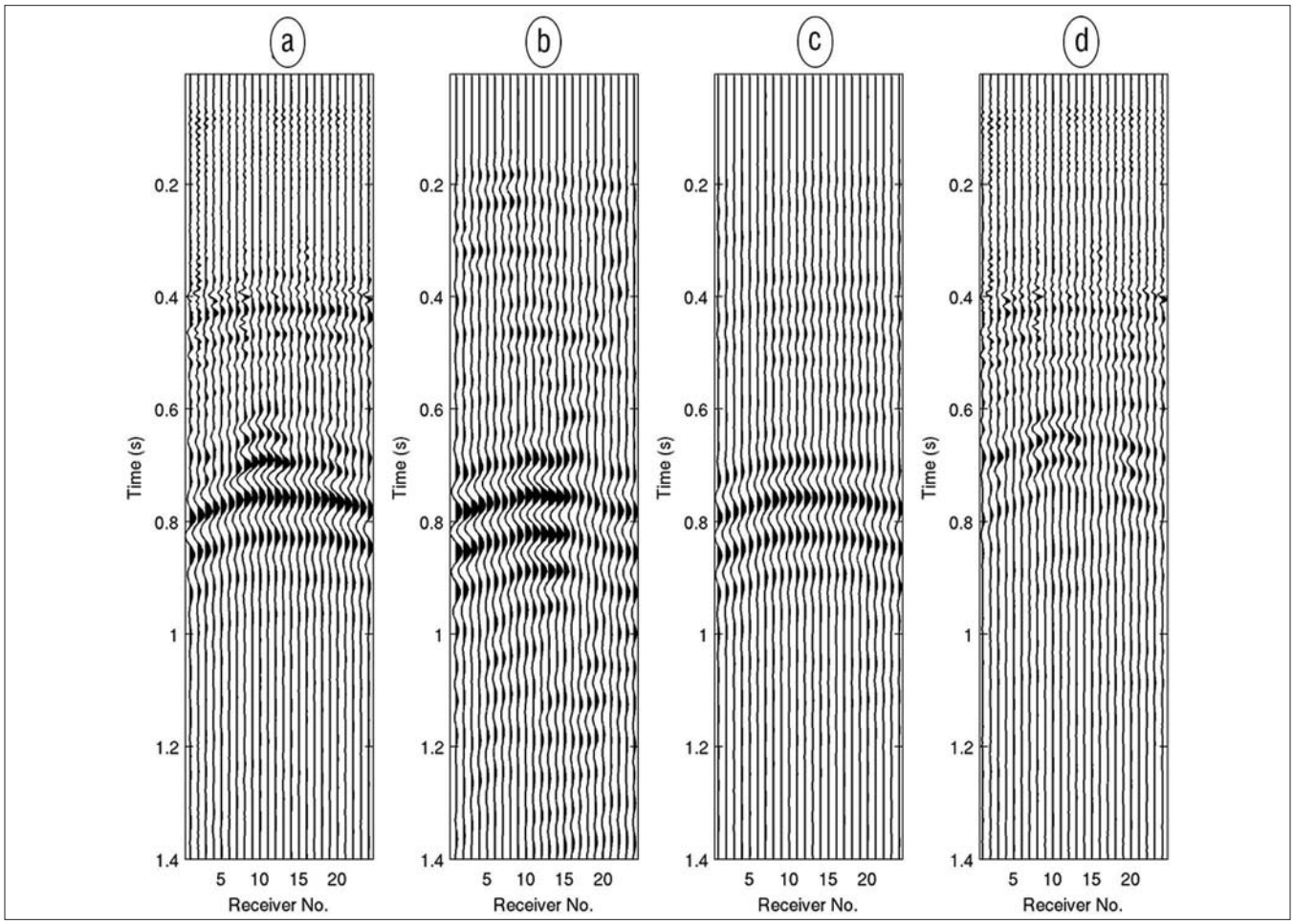

Figure 4. *Illustration of adaptive subtraction of source-receiver surface-wave estimates applied to data recorded on the 24-geophone linear array. (a) Data recorded from an active source at position* $\mathbf{r}_1$ *in Figure 2. (b) The source-receiver estimate with virtual source at position* $\mathbf{r}_1$*. (c) Surface-wave estimate as a result of adaptively matching the data in (b) to the data in (a). (d) Plot (a) minus plot (c). Receiver number increases towards the east. In all cases, a high-pass frequency filter with corner frequency of 10 Hz has been applied before plotting (a) and before both interferometry and further data processing of (b), (c), and (d).*

posed as a potentially useful technique in estimating and subsequently attenuating surface waves from seismic data. In the context of noise attenuation for land-based exploration seismology, this method is commonly referred to as interferometric ground-roll removal (Curtis et al., 2006; Dong et al., 2006; Curtis and Halliday, 2010; Halliday et al., 2010; van Wijk et al., 2010). The method takes advantage of the observed dominance of surface waves (ground roll) in waveforms constructed via seismic interferometry in order to estimate and then adaptively subtract surface waves from conventionally recorded seismic shot gathers.

Using inter-receiver interferometry, this method requires collocated sources and receivers in a seismic experiment, whereby the receiver used in constructing the interferometric (surface wave) estimate must be close enough to a real source position in order to produce a valid surface-wave estimate for data recorded from that real source. Using source-receiver interferometry, collocated sources and receivers are not required because the interferometric construction creates a virtual source directly from the real source itself, allowing a surface-wave estimate to be produced via interferometry for a source at the exact location of that used to acquire the real shot record. A drawback of using source-receiver interferometry in the application of interferometric ground-roll removal is the requirement of having two appropriate boundaries (see Figure 1) compared to the one boundary required for inter-receiver interferometry.

Figure 4 illustrates the adaptive subtraction of surface waves estimated using source-receiver interferometry from data recorded on the linear array from a real source at position $\mathbf{r}_1$ in Figure 2. Figure 4a depicts data (preprocessed as described above) as recorded by each receiver on the 24 receiver linear array from a real source at $\mathbf{r}_1$. The wavefield responses constructed by source-receiver interferometry are presented in Figure 4b. Note again the lack of high-frequency body waves in the source-receiver estimate. There is also some evidence of nonphysical energy in the source-receiver estimate upon comparison of Figures 4a and 4b.

The source-receiver interferometry result in Figure 4b is used as an estimate of the surface waves between position $\mathbf{r}_1$ and each linear array receiver. This estimate has then been adaptively subtracted from the data shown in Figure 4a using the method of Halliday et al. The adaptively filtered surface-wave estimate (Figure 4c) principally contains directly

propagating surface waves. The final result of the adaptive subtraction process (Figure 4d) contains little evidence of the lowest-frequency (approximately 10–20 Hz) surface waves arriving between 0.75 and 0.9 s. The slightly higher-frequency (approximately 20–30 Hz) arrivals around approximately 0.7 s are not well recovered in the source-receiver interferometry result (Figure 4b), and thus persist in the final result (Figure 4d).

Conclusions

This paper describes the first real-data application of the new, source-receiver form of interferometry. The example demonstrates that source-receiver interferometry enables the removal of directly-propagating surface waves using similar algorithms to previous studies that used inter-receiver interferometry (Curtis et al., 2006; Dong et al., 2006; Halliday et al., 2007; Curtis and Halliday, 2010; Halliday et al., 2010; van Wijk et al., 2010). The advantage of source-receiver interferometry is that receivers and sources do not need to be collocated; the disadvantage is the requirement for an extra boundary of sources or receivers compared to the inter-receiver or inter-source methods. The positive comparison of the performance of source-receiver interferometry versus the other two methods when constructing Green's function estimates from real data provides further evidence of the future potential of source-receiver interferometry. TLE

References

Bakulin, A. and R. Calvert, 2004, Virtual Source: new method for imaging and 4D below complex overburden: 74th Annual International Meeting, SEG, Expanded Abstracts, 2477–2480.

Curtis, A., 2009, Source-receiver seismic interferometry: 79th Annual International Meeting, SEG, Expanded Abstracts, 28, 3655–3659.

Curtis, A., P. Gerstoft, H. Sato, R. Snieder, and K. Wapenaar, 2006, Seismic interferometry—turning noise into signal: The Leading Edge, **25**, no. 9, 1082–1092, doi:10.1190/1.2349814.

Curtis, A. and D. Halliday, 2010, Source-receiver wavefield interferometry: Physical Review E: Statistical, Nonlinear, and Soft Matter Physics, **81**, no. 4, 046601, doi:10.1103/PhysRevE.81.046601.

Curtis, A., H. Nicolson, D. Halliday, J. Trampert, and B. Baptie, 2009, Virtual seismometers in the subsurface of the Earth from seismic interferometry: Nature Geoscience, **2**, no. 10, 700–704, doi:10.1038/ngeo615.

Dong, S., R. He, and G. Schuster, 2006, Interferometric prediction and least squares subtraction of surface waves: 76th Annual International Meeting, SEG, Expanded Abstracts, 2783–2786.

Forghani, F. and R. Snieder, 2010, Underestimation of body waves and feasibility of surface-wave reconstruction by seismic interferometry: The Leading Edge, **29**, no. 7, 790–794, doi:10.1190/1.3462779.

Halliday, D., and A. Curtis, 2008, Seismic interferometry, surface waves and source distribution: Geophysical Journal International, **175**, no. 3, 1067–1087, doi:10.1111/j.1365-246X.2008.03918.x.

Halliday, D. and A. Curtis, 2010, An interferometric theory of source-receiver scattering and imaging: Geophysics, **75**, no. 6, SA95–SA103, doi:10.1190/1.3486453.

Halliday, D. F., A. Curtis, J. O. A. Robertsson, and D.-J. van Manen, 2007, Interferometric surface-wave isolation and removal: Geophysics, **72**, no. 5, A69–A73, doi:10.1190/1.2761967.

Halliday, D. F., A. Curtis, P. Vermeer, C. Strobbia, A. Glushchenko, D.-J. van Manen, and J. O. A. Robertsson, 2010, Interferometric ground-roll removal: Attenuation of scattered surface waves in single-sensor data: Geophysics, **75**, no. 2, SA15–SA25, doi:10.1190/1.3360948.

Poliannikov, O.,2011, Retreiving reflections by source-receiver wavefield interferometry, Geophysics, **76**, no. 1, SA1–SA8.

Snieder, R., 2004, Extracting the Green's function from the correlation of coda waves: a derivation based on stationary-phase: Physical Review E: Statistical, Nonlinear, and Soft Matter Physics, **69**, no. 4 Pt 2, 046610, doi:10.1103/PhysRevE.69.046610.

van Manen, D.-J., A. Curtis, and J. O. A. Robertsson, 2006, Interferometric modeling of wave propagation in inhomogeneous elastic media using time reversal and reciprocity: Geophysics, **71**, no. 4, SI47–SI60, doi:10.1190/1.2213218.

van Wijk, K., D. Mikesell, T. Blum, M. Haney, and A. Calvert, 2010, Surface-wave isolation with the interferometric Green tensor: 80th Annual International Meeting, SEG, Expanded Abstracts, **29**, 3996–4000.

Wapenaar, K. and J. Fokkema, 2006, Green's function representations for seismic interferometry: Geophysics, **71**, no. 4, SI33–SI46, doi:10.1190/1.2213955.

Acknowledgments: Schlumberger Cambridge Research and the Natural Environment Research Council are thanked for their generous support of this research. Many thanks go to Ed Kragh, Everhard Muyzert, Gavin Menzel-Jones, Jim Smith, and Colin Kay for their assistance in data acquisition. Craig Duguid was at the University of Edinburgh when this work was carried out.

Corresponding author. Craig.duguid@tullowoil.com